

# The behavior of the active modes of the anatase phase of TiO<sub>2</sub> at high temperatures by Raman scattering spectroscopy

A Shirpay\*  and M Tavakoli

Department of Physics, Center of Basic Sciences, Khatam Ol-Anbia (PBU) University, Tehran, Iran

Received: 26 November 2020 / Accepted: 17 April 2021 / Published online: 20 May 2021

**Abstract:** In situ Raman spectroscopy is an important tool for describing the actual phase transfer conditions in metal oxides and provides important insights into the phase transition mechanism. The particle size, non-stoichiometry, and surface stress are well-known factors in the shifting and broadening of Raman modes for the TiO<sub>2</sub> anatase phase with increasing the temperature. Also, anharmonic effects in the form of phonon–phonon coupling and optical-phonon coupling are other factors in the shifting and broadening of Raman modes at high temperatures. In this paper, TiO<sub>2</sub> nanocrystals in the anatase phase are synthesized by the sol–gel method. Then the structure and size of the particles are investigated using XRD diffraction and SEM. Meanwhile, the contribution of phonon–phonon coupling for the third- and fourth-order has been studied for the active modes E<sub>g</sub>, A<sub>1g</sub>, and B<sub>1g</sub>, with increasing temperature (from room temperature to 943 K). The results of the back-scattering of in situ Raman spectroscopy show that the contribution of phonon–phonon coupling for the third-order has a significant effect on the shifting and broadening of Raman active modes. Also, the 412 cm<sup>-1</sup> mode behavior differs from the other two modes in the contrast between anharmonic couplings contribution and pure-volume contribution.

**Keywords:** Raman scattering; High temperature; TiO<sub>2</sub> nanoparticles; Anatase; Phonon–phonon coupling

## 1. Introduction

Raman spectroscopy is a sensitive technique used to study the structures of metal oxides, in the bulk phases or supported-surface phases, because it directly probes the vibrations of the bonds as well as the behavior of the metal-oxygen bond in the oxide structure [1]. Titanium oxide is used in various areas such as energy storage, medical devices, and catalytic surfaces [2–5]. TiO<sub>2</sub> phases are usually active Raman in the range of 100–900 cm<sup>-1</sup> [6–8].

Nanocrystalline TiO<sub>2</sub> has three main phases: the anatase phase which has a body center tetragonal structure and belongs to the (I4<sub>1</sub>/amd) D<sub>4h</sub><sup>19</sup> space group; the rutile phase of the tetragonal structure belonging to the D<sub>4h</sub><sup>14</sup> space group; and brookite phase which has less symmetry than the previous two phases and belongs to D<sub>2h</sub><sup>15</sup> space group [9, 10]. The catalytic activity of the anatase phase is appropriate because its Fermi level is about 0.1 eV higher than that of the rutile [11]. A mixture of 70% anatase and

30% rutile is the best photocatalyst for the oxidation of organics in the treatment of wastewater [12]. One of the main differences between the anatase and rutile phases is in the symmetry of oxygen atoms as well as the polarization of oxygen ions in which the oxygen vacancy creates Ti<sup>3+</sup> defect sites. These defects are of high importance in photocatalytic properties. In the TiO<sub>2</sub> photocatalytic application, the presence of unsaturated Ti<sup>3+</sup> ions plays an important role in the photo-oxidation of organic species [13].

Group theory shows that there are 69 optical modes for the brookite phase represented by 9A<sub>1g</sub> + 9B<sub>1g</sub> + 9B<sub>2g</sub> + 9B<sub>3g</sub> + 9A<sub>1u</sub> + 8B<sub>1u</sub> + 8B<sub>2u</sub> + 8B<sub>3u</sub> from which 36 modes (A<sub>1g</sub>, B<sub>1g</sub>, B<sub>2g</sub>, and B<sub>3g</sub>) are Raman active and the rest are active in infrared except A<sub>1u</sub>, which is inactive both in Raman and infrared [14]. For the anatase phase, there are 15 normal optical vibration modes A<sub>1g</sub> + 1A<sub>2u</sub> + 2B<sub>1g</sub> + 1B<sub>2u</sub> + 3E<sub>g</sub> + 2E<sub>u</sub> [15], from which six modes A<sub>1g</sub>, 2B<sub>1g</sub>, and 3E<sub>g</sub> are symmetric and active in Raman. In the rutile phase, 15 vibration modes A<sub>1g</sub> + 1A<sub>2g</sub> + 1A<sub>2u</sub> + 1B<sub>1g</sub> + 1B<sub>2g</sub> + 2B<sub>1u</sub> + 1E<sub>g</sub> + 3E<sub>u</sub> exist, where the B<sub>1g</sub>, E<sub>g</sub>, A<sub>1g</sub> and B<sub>2g</sub> modes are symmetric and active in Raman [7]. E<sub>g</sub>, B<sub>1g</sub>, and A<sub>1g</sub> Raman modes are related to symmetric bending

\*Corresponding author, E-mail: Ali\_shirpaei@yahoo.com

vibration and anti-symmetric bending vibration of O–Ti–O bonding, respectively [16, 20]. It has been reported by researchers that the observation of vibrational modes depends on the type of test and the test device used [8, 16–22]. The intensity of Raman's modes depends on the crystallizing mechanisms, which change with parameters such as pressure and temperature during phase formation. Also, the positions of Raman's modes vary with crystal size as well as various experiments [8, 16]. Various factors have been identified that affect the broadenings and shifting in the Raman modes of nanocrystalline TiO<sub>2</sub> in the anatase phase. The main factors can be summarized as follows:

*Effect of particle size:* TiO<sub>2</sub> nanoparticles have been frequently studied by Raman spectroscopy due to the unusual expansion and shift of the Raman modes when particle size decreases [23–26]. In these investigations, they used a model based on phonon confinement to explain the reason for the shift of the Raman modes. Based on Heisenberg's uncertainty principle, the relationship between particle size and phonon position can be expressed as follows:

$$\Delta X \Delta P \geq \frac{\hbar^2}{4} \quad (1)$$

where  $\Delta X$  is the particle size,  $\Delta P$  is the phonon momentum distribution and  $\hbar$  is the reduced Planck's constant. As the particle size decreases, the phonon is confined and the phonon momentum distribution increases. The broadening of the phonon momentum leads to a broadening of the scattered phonon momentum according to the momentum conservation law. The phonon dispersion causes asymmetric broadening and may lead to Raman bands shift [27]. The confinement of the phonon causes the breakdown of the phonon momentum selection rules. In other words, the  $q \approx 0$  phonons are active all over the Brillion zone of Raman, and the phonons are scattered throughout the Brillion region [28]. Also, asymmetric broadening and shift of Raman modes by decreasing particle size can be seen more for nanoparticles smaller than 10 nm. For example, Bassi et al. [22] observed the Eg (144 cm<sup>-1</sup>) mode shift in the anatase phase for nanocrystals with a size of less than 10 nm, in which the Raman modes shift to lower wavelengths by increasing the size of the nanocrystals. This shift was interpreted based on the phonon quantum confinement model.

*Stoichiometry:* Another factor in the unexpected shift of Raman modes is the appearance of a defect due to the oxygen vacancy. Non-stoichiometry strongly affects the vibrations of the lattice and changes the shape of the Raman spectrums in the oxides. When the samples have a lattice defect, the Raman modes generally become weaken and broaden [29]. Also, defects as the oxygen vacancies

shift the Fermi surface to the edge of the transmission band, increasing conduction [30]. At the nanoscale, the presence of oxygen vacancies is very significant for Raman's characteristics. It is difficult to assess the role of stoichiometry, especially in nanocrystalline systems, due to the quantitative determination of the ratio [O]/[Ti]. Annealing in air atmosphere reduces the deviation ratio from the [O]/[Ti] = 2. Therefore, due to the inhomogenous oxygen vacancies in the crystal lattice, the determination of the broadening and shift of the Raman spectrum caused by stoichiometry cannot be inferred [31, 32].

In studies of stoichiometry, Kumar et al. [13] observed stoichiometry effects, ranging from TiO<sub>1.89</sub> to TiO<sub>2</sub>, as-prepared samples in gas-phase condensation. Samples of titania had an oxygen deficiency and stoichiometric when annealed in air. Kumar did not report a complete list of all the possible Raman shifts by increasing the non-stoichiometry, believing that a similar shift would occur, and that the effects of crystal size and non-stoichiometry would be small, and that the particle size effect would be negligible compared to non-stoichiometry effect [33].

*Surface stress:* For small spherical particles, if  $P_i$  is the internal pressure and  $P_e$  is the external pressure, the increase in pressure  $P = P_i - P_e$  is applied horizontally or vertically as follows:

$$\Delta P \propto f/d \quad (2)$$

where  $f$  is the surface stress and  $d$  is the linear dimension of the particle. The concept of surface stress is applied at the surface of solids and is related to the free energy of the surface ( $\sigma$ ), which is an important part of the free energy of all nanoparticles. Free surface energy is defined as the reversible work per unit area surface or force per unit length in the formation of a new surface of nanoparticles [34]. However, the surface area of solids may change elastically with the deformation of the surface, assuming that the position of the lattice constants remains constant. In this case, the work per unit area surface or force per unit length is expressed by the following equation:

$$f = \sigma + A \frac{d\sigma}{dA} \quad (3)$$

Where  $f$  is the surface stress,  $A$  is the surface area,  $dA$  is the increase in the surface area in isotropic conditions, and  $\sigma$  is the free energy of the surface. In Equation (2) for bulk grains, the additional pressure of  $\Delta P$  due to the inverse dependence on the grain size is considered. In spherical particles with diameter  $d$ , the amount of additional pressure from relation (1) can be rewritten as follows:

$$\Delta P = \frac{4f}{d} \quad (4)$$

Therefore, phonon confinement, non-stoichiometry, as

well as surface stress play an important role in shift Raman modes. It should be noted that there are different beliefs about the effect of particle size and non-stoichiometry on the shift and broadening of Raman modes. For example, Choudhury et al. [35] studied TiO<sub>2</sub> nanocrystalline and found that by reducing oxygen deficiency, broadening of Raman's main mode was redshift, and by increasing annealing temperature and crystal size, Raman mode width decreased while Šćepanović et al. [36] believe that broadening and blueshift for the main mode (E<sub>g</sub>) occur at low temperatures, and at high temperatures the anharmonic effect is predominant and the phonon confinement effect decreases with increasing temperature. Zhang et al. [37] believe that the non-stoichiometry effect at higher frequencies of the rutile phase is negligible but has no effect on the main mode frequency (E<sub>g</sub>) of the anatase phase and also Ekoi et al. [38] increased the pressure from 1 kPa to 2 kPa; a shift in the Raman E<sub>g</sub> and A<sub>1g</sub> modes was observed, which occurs at lower wavelengths, but at higher pressures (3-5 kPa) the Raman mode shift is not significant.

Therefore, it can be said that due to the interdependence of the three factors mentioned above, determining the contribution of these factors in the shift and broadening of Raman modes seems very difficult and even impossible. Therefore, researchers usually consider one of the factors and assess its role. At high temperatures, the effect of anharmonic effects [34, 35, 38–41] is the predominant effect on the broadening and shift of Raman modes, which is in the form of phonon–phonon coupling and optical-phonon coupling. Therefore, in this paper, after preparing TiO<sub>2</sub> nanoparticles in the anatase phase by the sol–gel method and its characterization using XRD and SEM, the role of phonon–phonon coupling in the broadening and shift of TiO<sub>2</sub> nanoparticle Raman modes has been studied using Raman spectroscopy by increasing temperature.

## 2. Experimental details

### 2.1. Materials

Tetrabutyl titanate ( $\geq 99.99\%$  purity from Sigma-Aldrich), hydrochloric acid ( $\geq 99.99\%$  Merck), ethanol ( $\geq 99.8\%$  Merck), and deionized water were used.

### 2.2. Synthesis TiO<sub>2</sub> nanocrystals

To synthesize the TiO<sub>2</sub> nanocrystal by sol–gel technique, tetrabutyl titanate Ti(OBU)<sub>4</sub> was used as the precursor material, ethanol as the solvent, and hydrochloric acid and water as the reaction catalyst. An important role in the creation of optimal nanocrystal is to accurately determine

the molecular ratios of these materials. The best ratio for TiO<sub>2</sub> nanocrystal is as follows [27]:

Ti (OBU)<sub>4</sub>: EtOH: HCl: H<sub>2</sub>O = 1: 15: 0.3: 4

Hydrolysis and polycondensation reactions were carried out in the water at room temperature.

The steps for synthesizing TiO<sub>2</sub> nanoparticles are shown in Fig 1. The important point in this synthesis is that the amount of water greatly increases the particle size, although it accelerates the reaction and reduces the time it takes for the solution to turn into a gel. For this reason, hydrochloric acid was first diluted with deionized water (12.5% acid) and used in solution, in which case the nanoparticles were much smaller than when water was used directly in the reaction.

The produced nanocrystallites were analyzed by X-ray diffraction and field emission scanning electron microscopy imaging. To investigate the phase transition, band broadening and shift of the Raman modes of the TiO<sub>2</sub> nanocrystallites at high temperatures, calculation of the sample at 673K was carried out. The final powder was converted to a tablet in disc form and a specific experimental setup (Fig 2) was designed to measure the back-scattering Raman spectroscopy at different temperatures ranging from room temperature to 943K. The produced tablet from nanocrystallites with a diameter of 1 cm was put on a circle holder at the end of a crucible tube inside a furnace. The setup allowed the detection of a small fraction of the scattered light at a small solid angle, from the sample surface. The in situ Raman spectra of the sample inside the furnace were recorded which were accompanied by increasing the sample temperature from the room up to 943K.

## 3. Characterization

The samples were characterized by X-ray diffraction (XRD), field emission scanning electron microscopy (FE-SEM), TESCAN Company, model: MIRA3, Raman spectroscopy by Thermo Nicolet dispersive Raman spectrometer in the spectral region of 2-4300 cm<sup>-1</sup>. The X-ray diffraction patterns of samples were recorded by D8 Advance Bruker system with Ni filtered using Cu K $\alpha$  ( $\lambda = 0.15406$  nm) radiation.

## 4. Results and discussion

### 4.1. X-ray diffraction results

The produced TiO<sub>2</sub> nanopowders in the anatase phase were investigated by XRD. The spectrometer was model 1480 XPert manufactured by Philips. A very typical XRD

**Fig. 1** Flowchart synthesis of TiO<sub>2</sub> nanocrystals in anatase phase

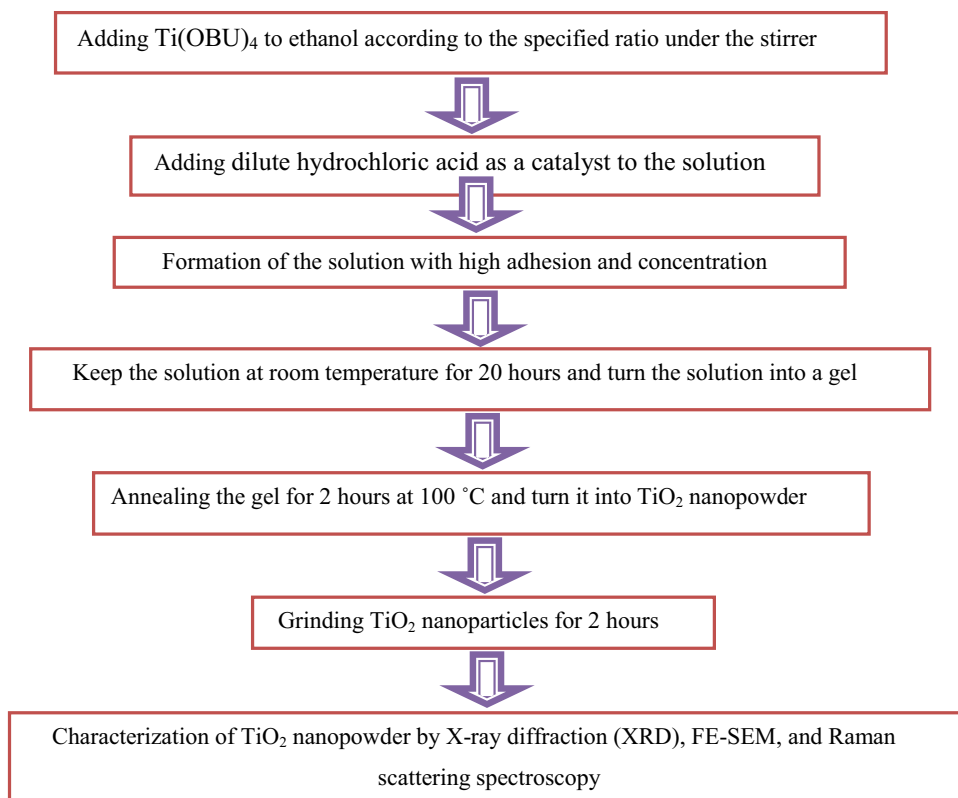


**Fig. 2** How to irradiate a laser beam on the TiO<sub>2</sub> anatase tablet in a furnace by increasing the temperature



pattern of the TiO<sub>2</sub> powders calcined at 673K is shown in Fig. 3.

According to the Debye–Scherrer formula, [40]:

$$D = k\lambda / \beta \cos\theta \quad (5)$$

the grain sizes of the synthesized particles were calculated to be in the order of 27.4 nm for the anatase phase. Diffraction line broadening is proportional to  $1/\cos\theta$  due to the crystallite size, while the broadening is proportional to  $\tan\theta$  due to the strains. The contribution of the strains to the broadening in the XRD patterns is smaller than that of the

crystallite size at low Bragg angles. It should be noted that in the estimation of the crystallite size by the Debye–Scherer equation, the strain contribution to the broadening was neglected; therefore, crystallite size will be smaller than the real size [42]. By increasing the temperature gradually, the anatase phase is transformed into a rutile phase. The approximation value for the weighted fraction of the rutile phase at one temperature can be calculated using the following expression [35]:

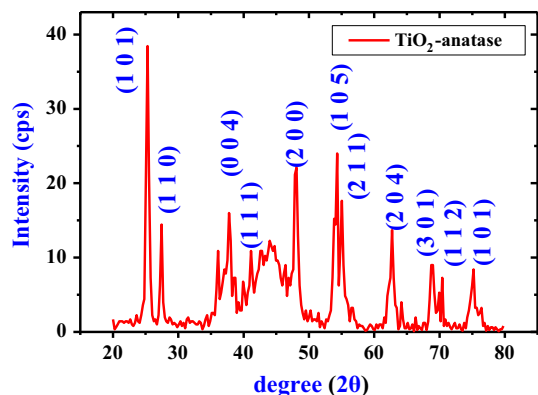


**Fig. 3** XRD pattern of the as-prepared anatase phase of  $\text{TiO}_2$  nanocrystals annealed at 673K

$$W_R = \frac{I_R}{0.884I_A + I_R} \quad (6)$$

Where  $W_R$  represents the weighted fraction of the rutile phase, and  $I_A$  is the integrated intensity of the anatase (101) peak and  $I_R$  is the integrated intensity of the rutile (110) peak. Using equation 6, the percentage of the rutile phase at 673K is about 30%.

#### 4.2. Morphology of nanoparticles by field emission scanning electron microscopy

To identify the morphology of  $\text{TiO}_2$  nanoparticles, FE-SEM emission scanning electron microscope, ARYA Electron (Philips) Company, and XL30 model were used.

The FE-SEM image of the sample (Fig4) shows the spherical morphology and particle size of the sample in the anatase phase. Since  $\text{TiO}_2$  in the anatase phase has a quadrilateral symmetry structure, the samples from the FE-

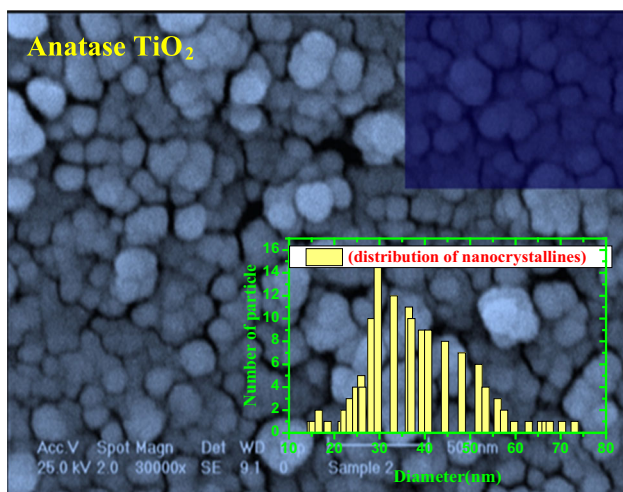


**Fig. 4** Morphology and histogram of the size distribution of the anatase phase of  $\text{TiO}_2$  nanocrystals at 673K

SEM images show that almost all of the nanoparticles in these images are seen separately or adhere together. As the temperature increases, the particle size increases and they transform from spherical to cubic in the rutile phase. The average particle size for the anatase phase was 35 nm, which is in good agreement with the results calculated with the Debye–Scherrer formula. However, the discrepancy in the determination of the nanocrystalline sizes by FE-SEM imaging and XRD patterns can be explained according to the sensitivity and physical principles of the applied experimental techniques. XRD patterns deal with a rather bulk crystalline sample, but SEM imaging focuses on a specific area of the crystalline surface.

$\text{TiO}_2$  nanocrystal in its anatase phase, with a good estimation, can be considered as a spherical shape and the distribution of particles can be determined at a certain temperature. Using particle size obtained from SEM imaging as well as SEM software, the particle size distribution can be roughly extracted. In this case, an SEM slide with about 300 particles was randomly chosen and using an Excel program, the nanocrystal size distribution is plotted with a typical diagram in Fig4. The graph shows the grain size distribution of  $\text{TiO}_2$  calculated at 773K in its anatase phase with a mean value of around 42 nm.

#### 4.3. Results of Raman spectroscopy

Understanding the origin of the different frequency shifts of Raman modes with increasing temperature can be categorized by the theory of lattice dynamics of anharmonic crystals. The treatments of anharmonic lattice dynamics are very complex, involving the techniques of many-body theory [34].

Anharmonic effects in the expansion of the potential function  $u = u_0^{\text{eq}} + u^{\text{har}} + u^{\text{anhar}}$  depend on temperature, and when anharmonic effects are examined, higher orders of expansion ( $n = 4$ ) should be considered. These effects play a role in the contraction and expansion of the crystal. Raman modes are a Lorentz function and, with a good approximation of up to 800 K, the four-phonon process is involved in the broadening and shift of Raman modes [35]. An approximate model can be considered to study the behavior of Raman's broadening and shift modes. For this purpose, the behavior of broadening and shift of frequency modes can be attributed to a first- or second-degree equation concerning temperature, and the broadening and shift of that specific phonon mode can be studied. So:

$$\omega = \omega_0 - \alpha_1 T - \alpha_2 T^2 \quad (7)$$

where  $\omega_0$  is the Raman shift when the temperature is extrapolated to 0 K,  $\alpha_1$  and  $\alpha_2$  are the first and second-order temperature coefficient.

The Raman shift dependence on temperature can be written as a result of two effects, one is the change in the vibrational frequencies due to the thermal expansion, and the other is due to the phonon anharmonic coupling with other phonons. Both of these effects have their origins in the disharmonious potential between the atoms. Due to the anharmonic of the specific Raman mode shift, the disorder can be separated as follows [43]:

$$\omega(T) = \omega_0 + \Delta^1(T) + \Delta^2(T) \quad (8)$$

where  $\Delta^1(T)$  represents the thermal expansion which is called a pure-volume contribution to the shift, and  $\Delta^2(T)$  is due to the anharmonic coupling. In this case,  $\Delta^1(T)$  can be expressed as [45]:

$$\Delta^1(T) = \Omega_0 \left[ \exp \left\{ -3\gamma \int_0^T \alpha(T') dT' \right\} - 1 \right] \quad (9)$$

where  $\Omega_0$  is the harmonic frequency of the optical mode and  $\gamma$  is the Grüneisen parameter for the optical Raman mode which is an important thermodynamic parameter in the study of pressure and temperature effects on physical and chemical properties of materials.  $\alpha(T)$  is the linear thermal expansion coefficient.

$\Delta^1(T)$  indicates independent non-normal frequencies of harmonic vibration in the expanded lattice, as a result of a volumetric expansion caused by temperature increase, which is usually attributed to the quasi-harmonic contribution. In most solids,  $\Delta^1(T) < 0$  which means the expansion as a result of softening.

The anharmonic coupling term  $\Delta^2(T)$  is due to the third-, fourth-, and higher-order anharmonic terms in the Hamiltonian, and it can be modeled as the following:

$$\Delta^2(T) = M_1 \left\{ 1 + \sum_{i=1}^2 \frac{2}{(e^{x_i} - 1)} \right\} + M_2 \left\{ 1 + \sum_{j=1}^3 \left[ \frac{3}{(e^{y_j} - 1)} + \frac{3}{(e^{y_j} - 1)^2} \right] \right\} \quad (10)$$

Where  $M_1$  and  $M_2$  are constant and are obtained by fitting these equations with the choice  $x_1 + x_2 = y_1 + y_2 + y_3 = \hbar\omega_0/k_B T$  in Eq. (7).

In  $\Delta^2(T)$ , the first term corresponds to the three phonon process (coupling or decaying of optical phonons into two phonons) and the second term corresponds to the four phonon process (coupling or decaying of three phonons and higher order). The three-phonon process is associated with the cubic term of the interatomic potential causing a negative frequency shift, whereas the shift associated with the quadratic anharmonicity is positive. Therefore, the resultant frequency shift due to the phonon-phonon interactions  $\Delta^2(T)$  may be either positive or negative depending on the

relative magnitudes of the anharmonic terms in the interatomic potential. Similarly, the Raman linewidth can be written as:

$$\Gamma(T) = N_1 \left\{ 1 + \sum_{i=1}^2 \frac{1}{(e^{x_i} - 1)} \right\} + N_2 \left\{ 1 + \sum_{j=1}^3 \left[ \frac{1}{(e^{y_j} - 1)} + \frac{1}{(e^{y_j} - 1)^2} \right] \right\} \quad (11)$$

Where  $x_i$  and  $y_i$  are defined in Eq. (10) and  $N_1$  and  $N_2$  are treated as fitting parameters. In the process of fitting equations, it is assumed that:

$$x_1 = x_2 = \frac{\hbar\omega_0}{2k_B T}$$

$$y_1 = y_2 = y_3 = \hbar\omega_0/3k_B T$$

Raman shift is usually the real part of the phonon self-energy and  $\Gamma(T)$  is equal to the phonon damping rate, which is the imaginary part of self-energy. Equation (11) is similar to Eq. (10), with the first term corresponding to the three phonon processes (which decays into two phonon processes), and the second term corresponding to the four-phonon processes (which decays into three phonons processes).

In calculating the shift and broadening of the Raman modes, the first anharmonic coupling is considered in the following form:

$$\omega(T) = \Omega_0 \left[ -3\gamma \int_0^T \alpha(T') dT' \right] + M_1 \left[ 1 + \frac{2}{(e^{x_i} - 1)} \right] + M_2 \left[ 1 + \frac{3}{(e^{y_j} - 1)} + \frac{3}{(e^{y_j} - 1)^2} \right] \quad (12)$$

where  $\Omega_0$  is obtained using the relationship:

$$\omega_0 = \Omega_0 + M_1 + M_2 \quad (13)$$

and  $\omega_0$  was given by extrapolating the fitting results to  $T = 0K$ [44–48].

Raman spectroscopy of the in situ samples of the TiO<sub>2</sub> nanoparticles in the anatase phase at different temperatures in the range of 300–943 K was recorded by a Thermo Nicolet dispersive Raman spectrometer in the spectral region of 2–4300 cm<sup>-1</sup>. Typical Raman spectra are shown in Fig. 5.

Fig 5 shows that all Raman modes are shifted and broadened as the temperature increases. As the temperature increases, bonds such as Ti–O, Ti–Ti, and Ti–O–Ti in the lattice structure of the anatase phase, depending on their site in the lattice structure, vibrate or change the type of bond, which causes phase transitions from anatase to brookite and rutile. As the temperature rises, the intensity of the peaks varies for different modes. Raman modes disappear almost at temperatures above 943 K. The first

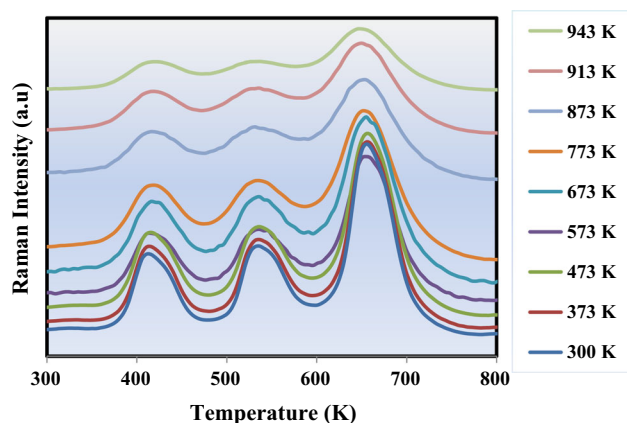


**Fig. 5** In situ high temperatures Raman spectra of the anatase phase of  $\text{TiO}_2$  nanocrystals

assumption is that since the transition to the rutile phase takes place near this temperature, the vibrations inside the lattice increase so much that all modes become too wide, so that, they cannot be seen separately.

The second assumption is that since the Raman spectroscopy test was performed at high temperatures, as the temperature rises to near 943 K, red light is emitted from inside the furnace, possibly affecting the scattered radiation from the sample.

Information on the shift and bandwidth of modes in the anatase phase of  $\text{TiO}_2$  sample from the in situ samples by increasing temperature shows that the strongest anatase peak ( $655 \text{ cm}^{-1}$ ) at room temperature with increasing temperature is shifted to higher frequencies ( $643 \text{ cm}^{-1}$ ) at 943 K, while at 913 K the  $534.9 \text{ cm}^{-1}$  mode shifts to  $535.5 \text{ cm}^{-1}$  and  $412.7 \text{ cm}^{-1}$  to  $420.8 \text{ cm}^{-1}$ . By increasing the vibrations of the lattice, shift, and broadening of the different modes of Raman, the behavior of each mode can be examined. The behavior of different modes of anatase phase and their bandwidth are given in Fig. 6 and Fig. 7 respectively.

As mentioned in the introduction, in addition to size effect, Stoichiometry, and surface stress factors, other factors such as optical-phonon or phonon-phonon coupling also contribute to the shift and broadening of Raman modes. To study the effect of optical-phonon or phonon-phonon coupling, the coefficients of equations (10) and (11) must be extracted. By fitting Eqs. (10) and (11) with the equations of shift and bandwidth of the Raman modes, the coefficients  $M_1$ ,  $M_2$ ,  $N_1$ , and  $N_2$  can be extracted, which are given in Table 1. During the fitting process, the Raman shift is very sensitive to the choice of  $M_1$ ,  $M_2$ , and  $N_1$ ,  $N_2$ .

Although the frequency changes of  $\text{TiO}_2$  Raman modes in the anatase phase with increasing temperature have been shown to have similar behavior in [46, 49], there is a slight difference with them. In the present study due to

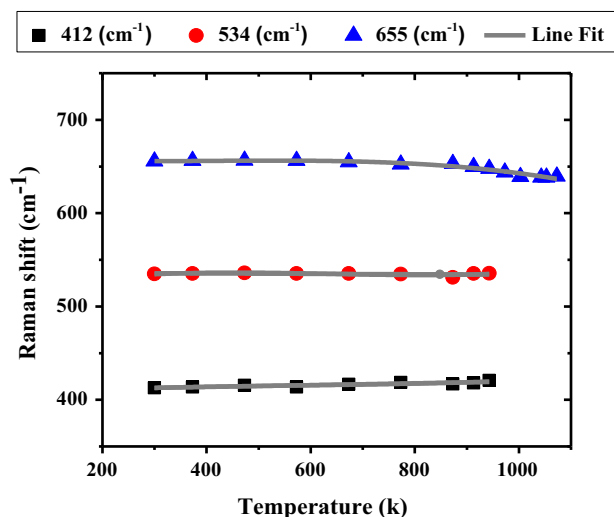


**Fig. 6** Raman modes shift of the anatase phase of  $\text{TiO}_2$  nanocrystals with increasing temperature

differences in the sensitivities of the device used, the lowest vibrational state of  $\text{TiO}_2$  ( $144 \text{ cm}^{-1}$ ) or due to the selection rules for the scattering geometry (Eg) or the limited rejection of the Rayleigh scattering radiation was not observed. The shift and bandwidth of Raman modes observed in this study are slightly different from [46, 49] due to the role of sentences in Equations 7 and 8, so that in [46] the Raman shift changes almost exponentially, and the bandwidth of Raman modes changes as sublinear. But in [49] the shift and bandwidth of Raman modes are almost linear. Therefore, it seems that the behavior of Raman modes in the present study has a high accuracy considering Eqs. 7 and 8.

Fig 6 shows that the behavior of all modes is almost linear. Table 1 also shows that the  $M_1$  and  $M_2$  signals are opposite, indicating that although the three-phonon process plays a dominant role in the temperature contribution, the four-phonon process is also required at higher temperatures. It is also observed that  $M_2$  is very small compared to  $M_1$ . Considering the net contribution of temperature in the shift of Raman modes, the three-phonon process plays a key role compared to the four-phonon process, intensifying the anharmonic couplings of optical phonons with increasing temperature. Due to the large value of  $M_1$  compared to  $M_2$ , it can be said that the role of the three-phonon process at higher temperatures is stronger than the four-phonon process. Of course, studies [34] have shown that  $\Delta^1(T) < 0$  is always present, but in contrast to the three-phonon and four-phonon process interactions, the result of the interaction may be positive or negative. Therefore, it can be said that in the interaction of  $\Delta^1(T)$  and  $\Delta^2(T)$ , if the result is positive, the phonon-phonon interaction process overcomes the thermal expansion

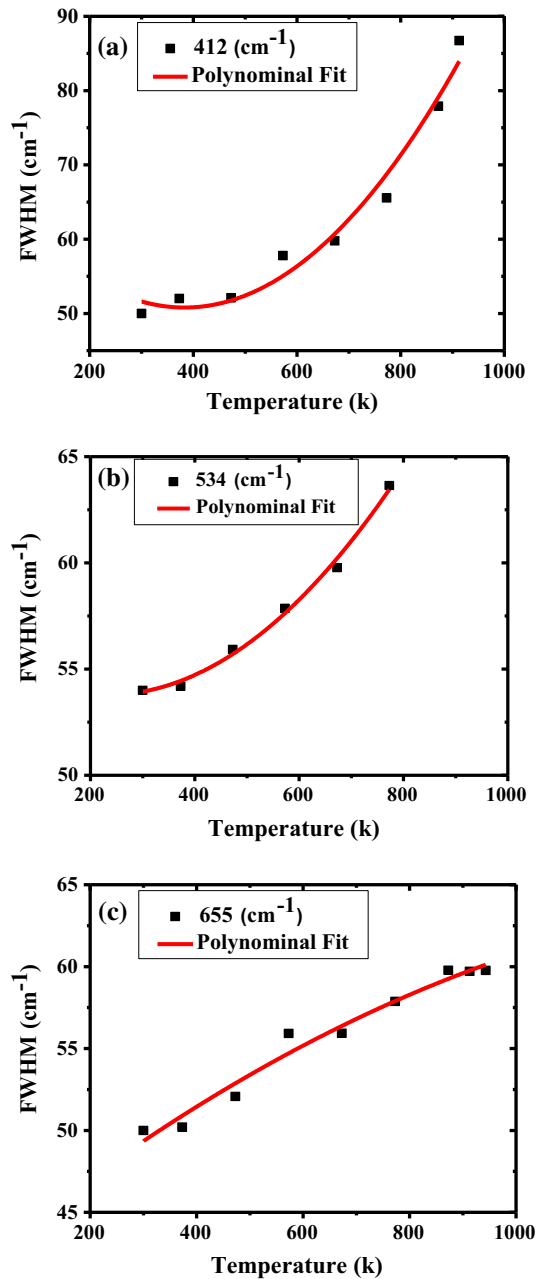


**Fig. 7** Full width at half maximum (FWHM) variation versus temperature in of the anatase phase of TiO<sub>2</sub> nanocrystals for different modes (a) 412 cm<sup>-1</sup>, (b) 534 cm<sup>-1</sup> and (c) 655 cm<sup>-1</sup>

**Table 1** Fitting parameters in the shift and broadening Raman modes in the anatase phase of dioxide titanium.

Modes (cm <sup>-1</sup> )	$\omega_0$ (cm <sup>-1</sup> )	$\alpha_1(\times 10^{-6})$	$\alpha_2(\times 10^{-4})$	$M_1$ (cm <sup>-1</sup> )	$M_2$ (cm <sup>-1</sup> )	$N_1$ (cm <sup>-1</sup> )	$N_2$ (cm <sup>-1</sup> )
E <sub>g</sub> (655.5 cm-1)	639.37	60	- 315	6.396	-0.021	- 6.744	0.025
A <sub>1g</sub> (534.9 cm-1)	534.97	4	- 4	0.226	-0.001	0.117	-0.001
B <sub>1g</sub> (412.7 cm-1)	411.23	-4	68	0.428	0.001	- 3.854	0.011

process. However, considering the positive slope of the 412 cm<sup>-1</sup> modes, it can be said that the anharmonic couplings contribution of this mode is more than the other two modes, and the pure-volume contribution is weak for this mode, but for the other two modes, the pure-volume contribution on the anharmonic couplings contribution dominates. This phenomenon can be attributed to the stronger phonon–phonon interaction of this mode than the other two modes, which is related to symmetric bending vibration of O–Ti–O bonding, but in the other two modes, the anti-symmetric bending vibration state of O–Ti–O bonding.

Fig 7 shows that Raman mode broadening behavior is a second-order equation with an increasing temperature that A<sub>1g</sub> mode behavior (534 cm<sup>-1</sup>) is different from the other two modes. This phenomenon can be attributed to the symmetric bending vibration E<sub>g</sub>, and B<sub>1g</sub> Raman modes and anti-symmetric bending vibration of O–Ti–O bonding.

Table 1 also shows that N<sub>2</sub> is very small compared to N<sub>1</sub>, meaning that the intensity of the contribution of phonon–phonon coupling for the fourth-order is weak. Large values of N<sub>1</sub> and  $\Gamma(0)$  indicate that the effect of the phonon–phonon coupling for the third-order is strong. This phenomenon is observed for all three modes B<sub>1g</sub> (412.4 cm<sup>-1</sup>), E<sub>g</sub> (661.1 cm<sup>-1</sup>), and A<sub>1g</sub> (536.6 cm<sup>-1</sup>). The behavior of the active Raman modes observed in this study is consistent with the modes in [46, 49] but differs slightly in the measured constant values.

## 5. Conclusions

In this paper, the effect of the temperature dependence of TiO<sub>2</sub> nanoparticles in the anatase phase on Raman active modes at high temperature was studied using experimental data. It was shown that the process of three phonons and four phonons coupling, as well as temperature expansion, sufficiently describes the shift and linewidth of Raman modes. The results obtained for TiO<sub>2</sub> nanoparticles in the anatase phase show that the behavior of all Raman modes is almost linear with increasing temperature. The results showed that the role of the three-phonon process is stronger



than the four-phonon process at higher temperatures. In  $412\text{ cm}^{-1}$  mode, the phenomenon of anharmonic couplings contribution overcomes pure-volume reduction, but for the other two modes, pure-volume reduction overcomes anharmonic couplings contribution. Raman mode broadening behavior with increasing temperature showed that the  $A_{1g}$  mode ( $534\text{ cm}^{-1}$ ) behavior is different from the other two modes, which seems to be due to the anti-symmetric bending vibration of O–Ti–O bonding.

## References

- [1] F D Hardcastle and I E Wach *J. Phys. Chem.* **95** 5031 (1991)
- [2] X Liu, P K Chu and C Ding *Mater. Sci. Eng. R Rep.* **47** 49 (2004)
- [3] A Fujishima and K Honda *Nature* **238** 37 (1972)
- [4] D A H Hanaor and C C Sorrell *Adv. Eng. Mater.* **16** 248 (2014)
- [5] D Kuciauskas, M S Freund, H B Gray, J R Winkler and N S Lewis *J. Phys. Chem. B* **105** 392 (2001)
- [6] G Deo et al *Appl. Catal. A Gen.* **91** 27 (1992)
- [7] S P S Porto, P A Fleury and T C Damen *Phys. Rev.* **154** 522 (1967)
- [8] I Lukačević, S K Gupta, P K Jha and D Kirin *Mater. Chem. Phys.* **137** 282 (2012)
- [9] H L Ma, J Y Yang, Y Dai, Y B Zhang, B Lu and G H Ma *Appl. Surf. Sci.* **253** 7497 (2007)
- [10] A Gajovic, M Stubicar, M Ivanda, K Furic *J. Mol. Struct.* **563** 315 (2001)
- [11] K Porkodi and S D Arokiamary *Mater. Char.* **58** 495 (2007)
- [12] K Zhua, M Sh Zhang, J M Honga and Z Yin *Mater. Sci. Eng.* **403** 87 (2005)
- [13] P M Kumar, S Badrinarayanan and M Sastry *Nanocrystalline Thin Solid Films* **358** 122 (2000)
- [14] G A Tompsett, G A Bowmaker, R P Cooney, J B Metson, K A Rodgers and J M Seakins *J. Raman Spectrosc.* **26** 57 (1995)
- [15] T Sekiya, S Ohta, S Kamei, M Hanakawa and S Kurita *J. Phys. Chem. Solids* **62** 717 (2001)
- [16] J Yan, G Wu, N Guan, L Li, Z Li and X Cao *Phys. Chem. Chem. Phys.* **15** 10978 (2013)
- [17] T Lan, X Tang and B Fultz *Phys Rev B* **85** 094305 (2012)
- [18] C R. Aita *Appl. Phys. Lett.* **90** 213112 (2007)
- [19] V Swamy, B C Muddle and Q Dai *Appl. Phys. Lett.* **89** 163118 (2006)
- [20] Y Zhang, C X Harris, P Wallenmeyer, J Murovchick and X Chen *J Phys Chem C* **117** 24015 (2013)
- [21] X Jiang et al. *J. Phys. Chem. C* **116** 22619 (2012)
- [22] A Li Bassi et al. *J. Appl. Phys.* **98** 074305 (2005)
- [23] V Swamy, A Kuznetsov, L S Dubrovinsky, R A Caruso, D G Shchukin and B C Muddle *Phys. Rev. B* **71** 184302 (2005)
- [24] D Machon et al. *J. Phys. Chem. C* **115** 22286 (2011)
- [25] Q Li et al. *Mater. Res. Bull.* **47** 1396 (2012)
- [26] D Machon, M Daniel, V Pischedda, S Daniele, P Bouvier and S LeFloch *Phys. Rev. B* **82** 140102 (2010)
- [27] N C Khang and N V Minh *J. Nonlinear Opt. Phys. Mater.* **17** 167 (2008)
- [28] S S Kanmani, N Rajkumar and K Ramachandran *Int. J. Nanosci.* **10** 227 (2011)
- [29] W F Zhang, Y L He, M S Zhang, Z Yin and Q Chen *J. Phys. D Appl. Phys.* **33** 912 (2000)
- [30] R Yew, S K Karuturi, J Liu, H H Tan, Y Wu and Ch Jagadish *Opt. Express* **27** 761 (2019)
- [31] L M Martínez Tejada, A Muñoz, M A Centeno, J A Odriozola *J. Raman Spectrosc* **47** 189 (2016)
- [32] B K Sarma, A R Pal, H Bailung and J Chutia *J. Alloys Comp.* **577** 261 (2013)
- [33] R J Gonzalez *Ph D Thesis* Virginia Tech (1996)
- [34] G R Hearne et al. *Phys. Rev. B* **70** 134102 (2004)
- [35] B Choudhury and A Choudhury *Int. Nano Lett.* **3** 55 (2013)
- [36] M J Šćepanović, M Grujić-Brojčin, Z D Dohčević-Mitrović, Z V Popović *Sci. Sinter.* **41** 67 (2009)
- [37] M S Zhang, Z Yin, Q Chen, X J Wu and X L Ji *Ferroelectrics* **168** 131 (1995)
- [38] E J Ekoi, A Gowen, R Dorrepaal, D P Dowling *Results Phys.* **12** 1574 (2019)
- [39] N T Sahrin, R Nawaz, Ch F Kait, S L Lee and M D Hakim *Wirzal Nanomaterials* **10** 128 (2020)
- [40] N S Yuksek and N M Gasanly *Cryst. Res. Technol.* **40** 264 (2005)
- [41] N M Gasanly, H Ozkan, A Aydinli, I Yilmaz *Solid State Commun.* **110** 231 (1999)
- [42] Z H Ni et al. *J. Raman Spectrosc* **38** 1449 (2007)
- [43] H Tang and I P Herman *Phys. Rev. B* **43** 2299 (1991)
- [44] A Gajovic, K Furic, N Tomasic, S Popovic, Z Skoko, S Music *J. Alloys Comp.* **398** 188 (2005)
- [45] W S Li, Z X Shen, Z C Feng and S J Chua *J. Appl. Phys.* **87** 7 (2000)
- [46] K Gao *Physica B* **398** 33 (2007)
- [47] M Maczka, J Hanuza, K Hermanowicz, A F Fuentes and K Matsuhiro *Z Hiroi J. Raman Spectrosc.* **39** 537 (2008)
- [48] Z D Mitrovic, Z V Popovic and M Scepanovic *Acta Physica Polonica A* **1** 116 (2009)
- [49] Y L Du, Y Deng and M S Zhang *J. Phys. Chem. Solids* **67** 2405 (2006)

**Publisher's Note** Springer Nature remains neutral with regard to jurisdictional claims in published maps and institutional affiliations.